Fracture Properties of Nanoclay-Filled Polypropylene

Ling Chen,[1] Shing-Chung Wong,[2] Sreekumar Pisharath[1]

[1]*School of Materials Engineering, Nanyang Technological University, Nanyang Avenue, Singapore 639798, Republic of Singapore*
[2]*Department of Mechanical Engineering and Applied Mechanics, North Dakota State University, Fargo, North Dakota 58105*

Received 27 March 2002; accepted 23 September 2002

ABSTRACT: Maleic anhydride-modified polypropylene was compounded with commercially available surface-modified montmorillonite in a twin-screw extruder. Recompounding ensured the removal of visible tactoids from the extrudate but TEM and XRD techniques showed nonuniform dispersion of clay platelets. In this study, we investigated the mechanical and fracture properties of nanoclay-filled polypropylene. Emphasis was placed on the fracture characterization of the clay-filled polypropylene. Tensile strength and stiffness increased steadily with an increase in the clay loading. The toughness of compounded materials was characterized using rigorous fracture mechanics. *J*-integral fracture resistance decreased with an increase in the clay content. The resistance against stable crack growth was compared using the slopes derived from the *J*–*R* curve and the tearing modulus concept. A significant amount of crack growth resistance was evident in the nanoclay-filled polypropylene as opposed to other brittle nanocomposites such as the nylon–clay systems. © 2003 Wiley Periodicals, Inc. J Appl Polym Sci 88: 3298–3305, 2003

Key words: poly(propylene) (PP); organoclay; fracture; toughness; nanocomposites

INTRODUCTION

Present efforts to investigate polypropylene (PP)-based nanocomposites are centered around uniformly dispersing modified clay particles in nonpolar matrices to maximize their physical and mechanical properties. Clay exfoliation was pursued using a mixture of stearyl ammonium-exchanged montmorillonite, maleated polypropylene (MAPP), and the PP homopolymer and dispersive mixing using extrusion compounding.[1–6] The attempt to fully exfoliate clay particles in PP has been fraught with challenges[7] due to the mismatch in surface polarity between the clay and the pristine polymers. Most dispersive mixing also requires an anhydride-modified PP oligomer[8–11] to compatibilize the clay and PP homopolymer. Nevertheless, nanolayer exfoliation in PP compares poorly to that of nylon–clay nanocomposites. The critical advantage of producing clay-filled PP composites is, however, often cited for its great processability and low cost to replace existing engineering and functional materials. They are attractive as packaging materials where enhanced barrier properties are desired. It is essential for PP nanocomposites to be capable of being mass produced for resin supplies in automotive and packaging industries. Some success in the mass-production route was recently reported,[5,12] whereby the clay was uniformly dispersed in the PP matrix by mechanical mixing as evident in transmission electron microscopy (TEM) micrographs.

Little is understood of the failure and fracture behaviors of nanoclay-filled polymers.[13,14] Most prior studies[1–11] were concerned with clay exfoliation in the matrix. Of particular interest to fracture behavior is the role played by the clay particles in nucleating or enhancing the localized crack tip stress fields. In this article, we report the mechanical and fracture properties of organoclay-filled PP. We used MAPP to promote better dispersion of clay in the PP matrix. Most of the polyolefin-based composites exhibited substantial elongation at break[5] in contrast to those pertaining to nylon-based systems, which were drastically embrittled by the presence of clay. It would be interesting to examine the fracture behavior[13,14] of such seemingly ductile composites using a rigorous fracture mechanics approach, which allows future modeling and detailed examination of the structure–fracture property relationship. *J*-integral fracture toughness was used to characterize the initiation toughness of the studied materials while the slopes of the *R* curves are indicative of the resistance against crack growth and the extent of geometry-dependent plastic deformation. TEM and X-ray diffraction (XRD) were used to provide information regarding the degree of clay agglomeration and exfoliation. Fracture surfaces were examined using scanning electron microscopy (SEM).

Correspondence to: S.-C. Wong (Josh.Wong@ndsu.nodak.edu).

Journal of Applied Polymer Science, Vol. 88, 3298–3305 (2003)

EXPERIMENTAL

The matrix material used in this study was maleic anhydride-modified PP (MAPP; Bynel 50E561) from DuPont (Singapore) Pte. Ltd. Its melt flow rate was 5.0 dg/min and the given melting point was 141°C from the manufacturer. The organoclay (Nanomer I.31PS onium ion-modified montmorillonite clay), which was-modified with octadecylamine, was supplied from Nanocor Inc. (USA).

MAPP and organoclay were melt-compounded in a corotating intermeshing twin-screw extruder (Leistritz Micro 18 $L/D = 30$). The compounding temperature was 210°C to produce the masterbatch containing 50 wt % clay, to be followed by recompounding with fresh MAPP resins in a temperature range of 185–210°C and a screw speed of 200 rpm to obtain clay-filled PP with lower loading levels of organoclay. The loadings were selected to give a broad profile of samples to identify the effect of clay on the fracture toughness of PP. The blended samples were reextruded again in the twin-screw extruder to achieve better dispersion. Materials were injection-molded into 3.5-mm-thick dumbbell specimens and 6.17-mm-thick single-edge notch-bend (SENB) specimens for fracture tests. All materials were dried at 80°C in a vacuum oven prior to compounding and injection molding.

The degree of intercalation and dispersion of the compounded clay-containing MAPP was examined using XRD and TEM. The extrudates were hot-compressed at about 170°C using glass slides on a hot plate and subsequently cooled with ice. Then, the thin sheets of the compressed extrudate and injection-molded tensile bars were, respectively, examined using a Rigaku wide-angle X-ray diffractometer at 40 kV/30 mA and the scanning rate was $2°\text{min}^{-1}$ at an interval of 0.02°. The tips of the extrudates were trimmed into smaller surfaces (0.3 × 0.3 mm) for ultrathin sectioning. Ultrathin sections were slowly cut at 0.2 mm s^{-1} from the surface perpendicular to the flow direction using a diamond knife with a Leica Ultracut UCT microtome at ambient temperature. The sections were collected on 200-mesh copper grids and dried with filter paper subsequently. A JEOL 2010 TEM operating at an accelerating voltage of 100 kV was used to examine the sections.

Tensile tests were conducted according to ASTM D638 using an Instron Model 5567 computer-controlled testing machine equipped with an extensometer. The crosshead speed was kept constant at 5 mm min^{-1} at ambient temperature. At least five specimens of each composition were tested. The *J–R* curves for the specimens were determined using deeply notched three-point bend specimens ($S/W = 4$, $L = 55$ mm, $W = 12.50$ mm, $B = 6.17$ mm). Precracks were made by inserting a fresh razor blade into the machined slot and the crack-to-width ratio, a/W, was limited to 0.50–0.65 in all tests. A multiple-specimen technique[15] was adopted to conduct the *J*-integral tests. In this method, one specimen from each of the compositions was loaded to complete failure and the load-deflection curves were obtained. The subsequent specimens from the compositions were loaded to different points in the load-deflection profile and unloaded. The unloaded specimens were fast-fractured after immersing them into liquid nitrogen for a minimum of 20 min. The amount of stable crack growth, Δa, was measured from the fracture surface using an optical microscope (Olympus BH-UMA) with a micrometer eyepiece attached. Stable crack growth and a large stress-whitened zone were observed for all specimens. The crosshead speed was 5 mm min^{-1} and tests were conducted at room temperature.

J_R was determined from

$$J_R = \frac{2U}{Bb} \tag{1}$$

where U is the area under the load versus the load point displacement curve and $b = W - a$ is the ligament length. The data for the J_R curve were best-fitted to a linear regression line and the intersection between the regression line and a 0.2-mm offset line, which is parallel to the blunting line, was used for evaluation of the initiation value of J as recommended by ASTM E1737-96. The initial slope of the *J–R* curve was quantified by a dimensionless tearing modulus T_R:

$$T_R = \frac{E}{\sigma_y^2}\frac{dJ_R}{da} \tag{2}$$

where E is the Young's modulus and σ_y is the yield stress of the material. The size requirements for the valid J_{Ic} of the SENB specimens were also checked with the relationship, $B, W - a \geq 25\, J_{Ic}/\sigma_y$.

SEM observations of the blends were performed on a JEOL 5410 LV Model SEM. Fractographic examinations were conducted on the specimen obtained from the *J*-integral tests. All specimens were coated with gold in an SPI sputter coater before SEM observation.

RESULTS AND DISCUSSION

Dispersion of organoclay in MAPP matrix

The XRD results for different blend compositions are shown in Figure 1. The clay-filled MAPPs at different weight fractions are compared to unfilled MAPP and clay alone. It is evident that the MAPP was able to intercalate into the galleries and caused the increase in *d*-spacing in the extruded samples. The peak position of pristine organoclay at $2\theta = 4°$ (2.2 nm) displayed by the solid line shifted to a smaller angle of $2\theta = 3.2°$ (2.7 nm) when the MAPP was reinforced with 20 and 30 wt

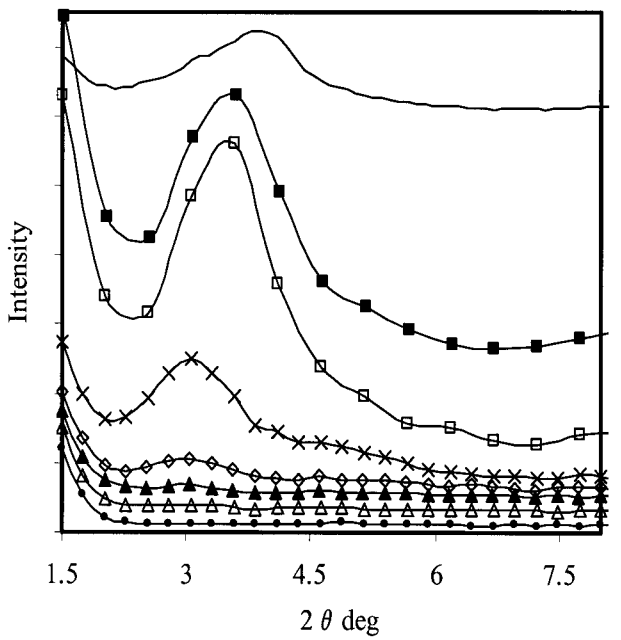

Figure 1 XRD data of the extrudates of nanoclay-filled PP containing (●) 0 wt %, (△) 5 wt %, (▲) 10 wt %, (◇) 20 wt %, (×) 30 wt %, (□) 40 wt %, (■) 50 wt %, and (—) 100 wt % clay.

% clay. The *d*-spacing for 40 and 50 wt % clay systems was, however, about 2.5 nm ($2\theta = 3.5°$), indicating that, at a higher clay content, the shift in the angle was minimal and clay agglomeration became severe. Note that the clay loadings were selected to investigate the broader profile of the effect of clay on the fracture toughness of PP. For MAPP containing a 5 and 10 wt % nanoclay content, there existed only very slight peaks in the XRD results from the extrudate, which suggests that the dispersion of clay at low concentrations was good. This result by no means verifies clay exfoliation as clay platelets could be disordered during compounding. Whether true nanocomposites were obtained through the recompounding process was viewed cautiously. We believe that the silence of the X-ray intensity exhibited by the low-concentration composites needs to be explained by polymer–clay intercalation instead of clay exfoliation. If the gallery spacing of clay momentarily exceeds the limit (≈8 nm) of the wide-angle X-ray (WAXD) used in this study, we would not have observed any peaks in Figure 1. The shear forces experienced by the extrudate in the twin-screw extruder could contribute to localized viscoelastic deformation like slipping between the clay galleries during melt processing and promote a disordered structure rather than exfoliated clay.

The silent XRD curve for the 5 wt % clay system is not reproducible when the extruded pellets are injection-molded. Figure 2 juxtaposes the XRD data of the extrudate and injection-molded sample following extrusion compounding. The two peaks displayed by the injection-molded specimen correspond to the *d*001 and *d*002 diffractions, respectively. It is understood that processing conditions play an important role in clay exfoliation and agglomeration.[6] We conjecture that the intercalated clay morphology revealed under high shear forces in the extruder was unstable prior to injection molding. Once the extruded pellets were reheated to the melting temperature, the shear stresses were relieved and the clay galleries regained their native dimensions.

To critically examine the dispersion of organoclay, TEM techniques were applied to the extrudates. Specimens were microtomed perpendicular to the melt-flow direction. The TEM micrographs of 10 and 50 wt % clay-filled MAPP at different magnifications are given in Figure 3. Clearly, the dispersion is not uniform, as we expected, and some microtactoids can be noted on these micrographs. The aggregates of clay are obvious at a 50 wt % clay content. Nevertheless, a number of nanometer-thick clay morphologies could be identified. The morphology at a low clay content (10 wt %) presents a mixture of intercalated and partially exfoliated features. The dispersion is better at a lower clay loading than at a high clay loading. This observation is consistent with the conclusion suggested by Pinnavaia et al.[16] The processing–structure relationships await future investigations.

Mechanical properties

All stress–strain behaviors of clay-filled MAPP displayed postyield elongation. The tensile yield strength and tensile modulus are plotted in Figures 4 and 5, respectively, as a function of the clay content. The yield strength was obtained from the intersection be-

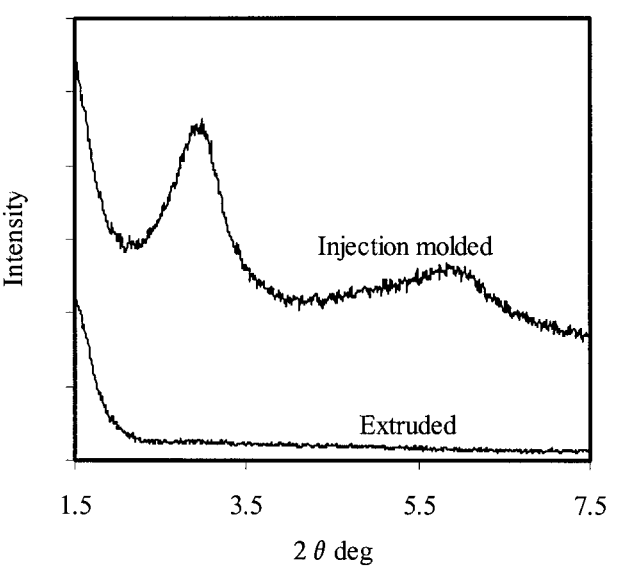

Figure 2 XRD of the extruded and injection-molded samples of clay-filled PP containing 5 wt % clay.

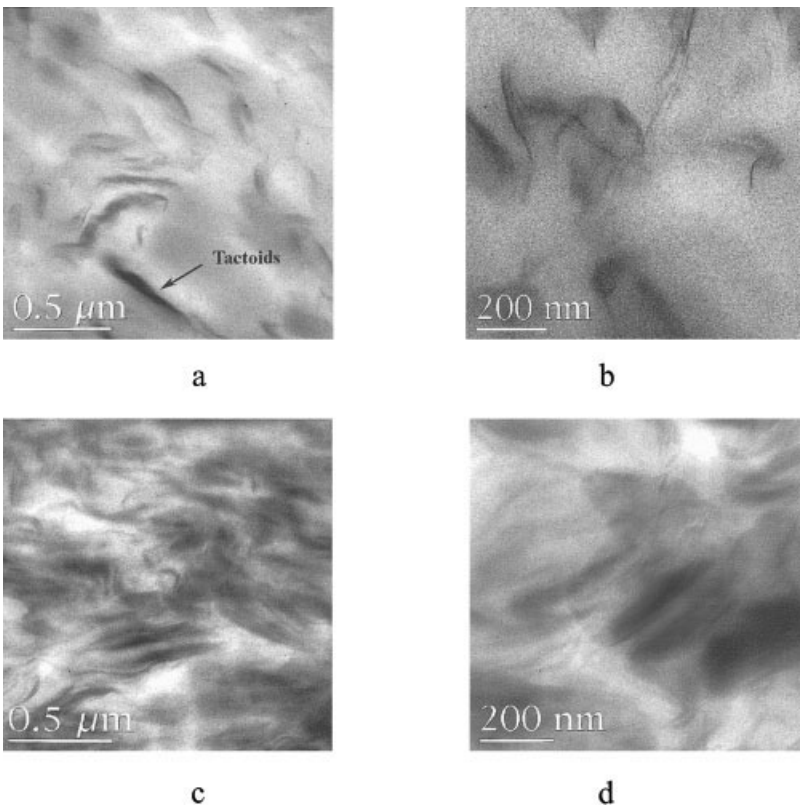

Figure 3 TEM photomicrographs of clay-filled PP containing (a) 10 wt % clay (low mag), (b) 10 wt % clay (high mag), (c) 50 wt % clay (low mag), and (d) 50 wt % clay (high mag).

tween the stress–strain curve and the tangent line at 0.2% strain offset. Both the yield strength (Fig. 4) and the tensile modulus (Fig. 5) increased with the clay content. It is noteworthy that the yield strength is double that of unreinforced MAPP, while the tensile modulus is sixfold that of unreinforced MAPP at 40 wt % clay. The role of the clay as a reinforcer in the MAPP matrix is evident. Nevertheless, the effectiveness of reinforcement remains unclear because the comparison of the experimental data at different weight fractions of clay with the volume-averaged relationship could not be conclusively ascertained. The latter requires a careful characterization of the tensile strength of clay particles at the same size scale of intercalated clay in the polymer matrix. At 30 wt % nanoclay and above, there exists a more distinctive

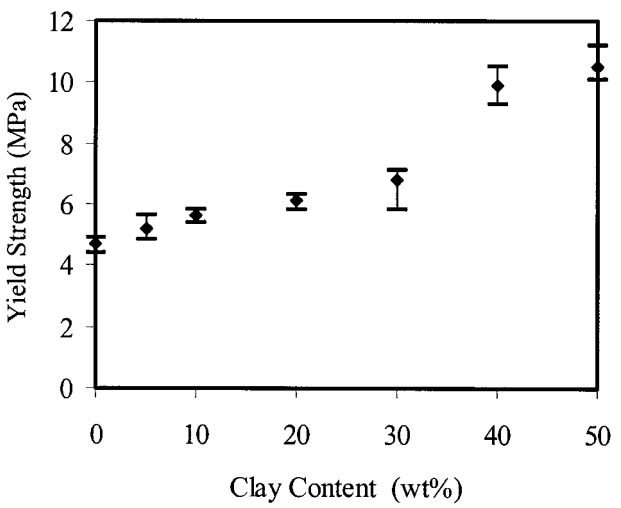

Figure 4 Yield strength of nanoclay-filled PP versus clay concentration.

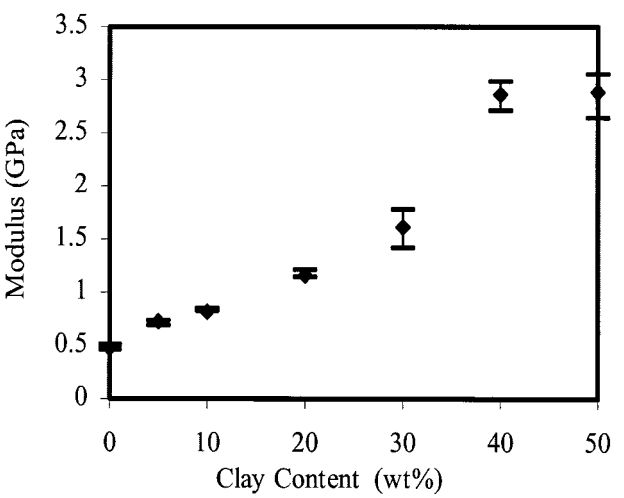

Figure 5 Elastic modulus of nanoclay-filled PP versus clay concentration.

increase in the tensile properties. The improvement in strength was quite gentle at a low clay content (5 and 10 wt %). The trend is consistent with the results reported by others.[7,17] According to Kojima et al.,[18] a region where the polymer chains are restricted in mobility contributes to the improvement of the tensile modulus in a polymer–clay hybrid. Increasing the clay content will greatly constrain the polymer chains' mobility so that the modulus is improved. Based on the fact that the improvement in mechanical strength and stiffness for clay-filled PP are not as drastic as in the nylon–clay systems,[18,19] we surmise that there is still much room for clay reinforcement in PP. An observed decrease in the elongation at break could be explained by the same reasoning because the plastic deformation of the polymer matrix is greatly limited by an increase in the clay loading. The detailed understanding of the interfacial adhesion between the clay and the polymer is lacking. The effect of clay dispersion in molecular chain confinement is not understood. However, we believe that the interfacial bonding between hydrophilic-layered silicates and hydrophobic PP is markedly weaker than that in nylon nanocomposites,[18,19] whereby a few weight percent of clay could deliver a multifold increase in strength and modulus. The mismatch in the surface polarity not only hinders the degree of dispersion of clay agglomerates in the organophilic PP but also limits the reinforcement effect arising from the much stronger clay.

Fracture behavior

This article focused on the fracture properties of organoclay-modified PP. While most studies in nanocomposites focus on improvements in the mechanical strength and moduli, heat-deflection temperature, barrier properties such as flame retardancy, moisture and oxygen resistance, etc.,[19–27] few[13,14] have provided comprehensive reports of the fracture behavior and properties of such novel composites. As they differ from microcomposites, which often fail by delamination and pose challenges for rigorous fracture characterization, one critical advantage of studying clay-filled engineering plastics using fracture mechanics is they could be treated similarly to continuum plastics because the size of the filler is comparatively smaller than other inorganic fillers such as short glass fibers. Unlike the fiber-reinforced polymers, the size of the clay particles is too small to bridge any crack faces. Any crack growth resistance needs to be explained in terms of matrix-driven deformation mechanisms. We attempted using *J*-integral analysis on the clay-filled PP in this study in view of the extensive postyield deformation demonstrated by polyolefin-based nanocomposite systems. The fracture initiation toughness was determined following ASTM E1737-96 in which a blunting line solution at a 0.2-mm offset is used for evaluation of the initiation value of *J*.

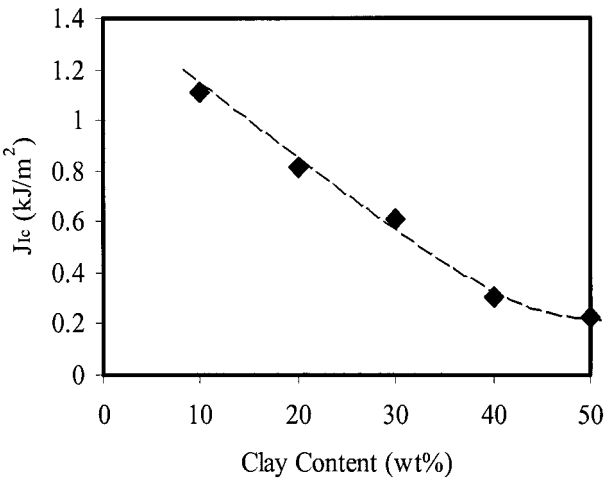

Figure 6 J_{Ic} of nanoclay-filled PP versus clay content. The *J*-integral fracture resistance of unfilled MAPP does not satisfy the thickness conditions for plane-strain toughness.

Figure 6 plots the *J*-integral initiation toughness resistance versus the clay content. However, after checking the size requirements for valid J_{Ic}, only the *J*-integral fracture resistance of 6.17-mm-thick unfilled MAPP specimens could not satisfy the plane strain conditions and J_c = 4.14 kJ/m^2 for 0 wt % clay. The fracture initiation toughness decreases with the addition of clay as shown in Figure 6. Upon the addition of 10 wt % clay, the fracture initiation toughness decreases to one-fourth the matrix toughness. J_{Ic} decreases steadily with an increase in clay loading thereafter. The trend in toughness appears opposite to that of the increase in strength and stiffness. This is understood if the effect of chain confinement limits intrinsic polymer deformation.

Figure 7 shows SEM photomicrographs of the clay-filled MAPP. Figure 7(a–f) shows a transition from ductile to brittle fracture. The fracture surface of unfilled MAPP [Fig. 7(a)] shows rather ductile features with extensive voiding and PP fibrous structures stretching over the crack face prior to fracture. While some degree of elongation and fibril formation of the PP domains could be observed with the introduction of 10 wt % clay [Fig. 7(b)], the fibrils appear much finer and premature voiding is now contained. The latter observation suggests that the presence of clay markedly hindered void formation during deformation and less PP was available for bridging the crack face. An increase of clay loading up to 20 wt % does not seem to alter the fracture surface in Figure 7(c) dramatically from Figure 7(b). However, some islands of clay agglomerates known as tactoids could be identified in Figure 7(c) at 20 wt % loading in the midst of extensively deformed PP fibrous structures. Matrix deformation is greatly reduced when the clay loading is

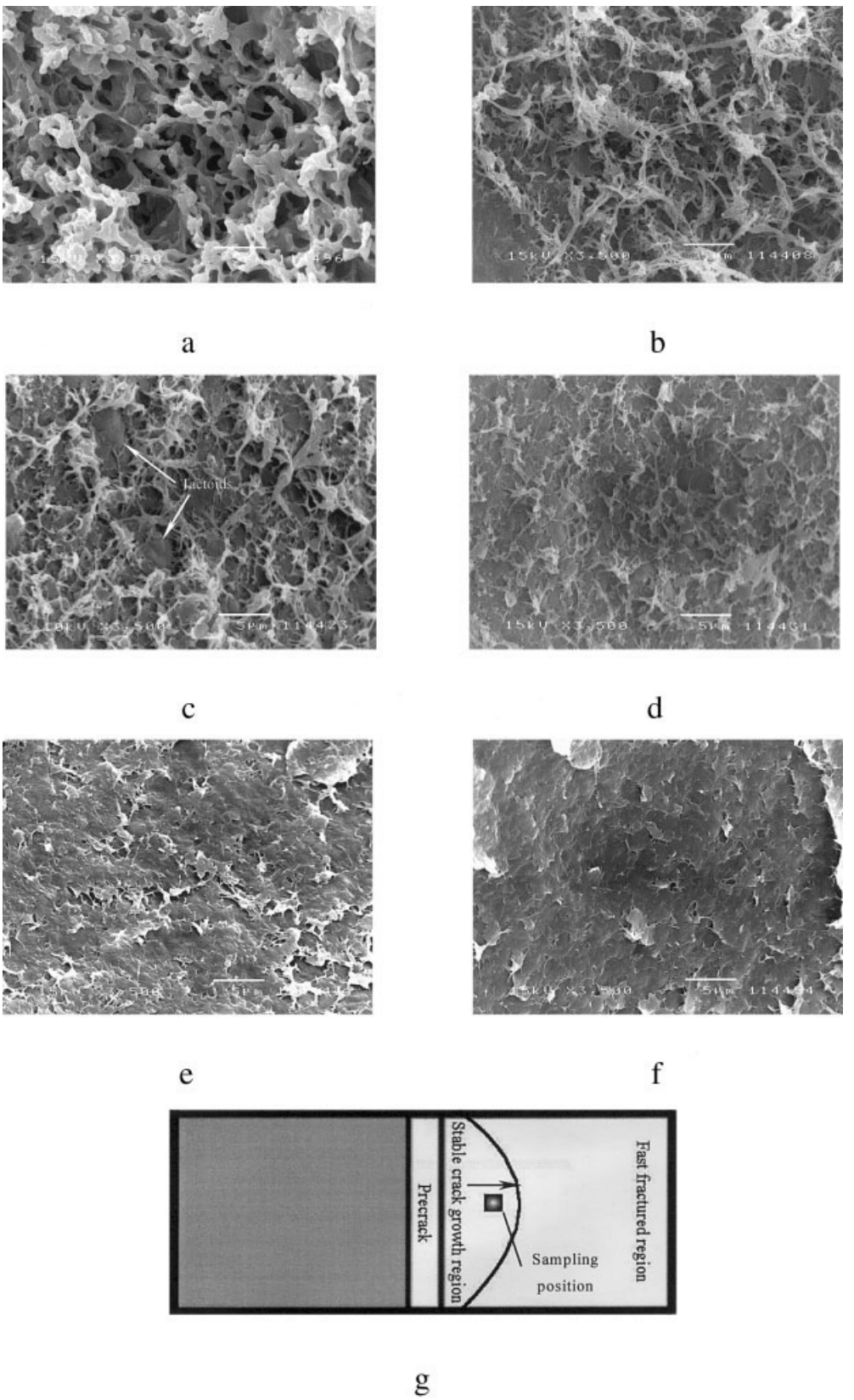

Figure 7 SEM photomicrographs of nanoclay-filled PP containing (a) 0 wt %, (b) 10 wt %, (c) 20 wt %, (d) 30 wt %, (e) 40 wt %, and (f) 50 wt % clay while (g) gives a schematic sampling position of the fracture surface under SEM observation. The arrow indicates the direction of crack propagation.

increased up to 30 wt %. Lumps of clay platelets could still be observed in Figure 7(d) despite that the contrast with deformed PP phase is now minimal. The fracture surface becomes featureless in Figure 7(e,f) as the matrix deformation is severely constrained in comparison to the compositions at lower clay loadings. Clearly, fracture behavior changes from a rather ductile matrix voiding and fibrous deformation to featureless brittle cleavage when clay loading increases. The fractographic results are consistent with the change in the *J*-integral fracture initiation toughness.

It is instructive to evaluate the fracture resistance against crack growth at least in the very beginning region of the *J–R* curve. Figure 8 shows the slopes of the initial *R* curves of each blend composition studied in this article. The pristine MAPP gives rise to the greatest slope as compared to other compositions at higher clay loading. Both 10 and 20 wt % clay systems provide relatively sharp slopes, which indicate a more substantial resistance against crack propagation. The slope starts decreasing most pronouncedly at a 30 wt % or higher loading of clay. However, all slopes indicate a rather strong *R*-curve behavior for nanoclay-filled PP. This point is noteworthy as nanoclay-filled plastics are expected to be highly embrittled by the presence of nanoscale fillers.

A plot of the tearing modulus, which incorporates the intrinsic stiffness and strength of the composites versus clay loading, is given in Figure 9. In all clay-filled MAPP, the 20 wt % loading produces the highest tearing modulus, which suggests that the composition possesses the best combination of stiffness and crack growth resistance, both of which are critical design parameters for enhancing the toughness of materials. The rather substantial tearing modulus indicates that the deformation mechanisms of nanoclay-filled PP systems could be complex. The interfacial bonding between the clay and the PP matrix suffices to produce

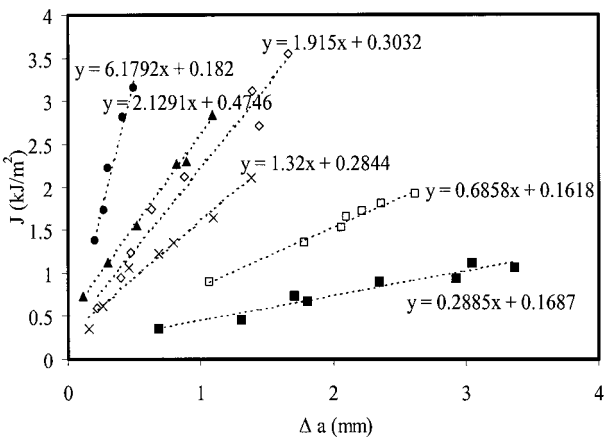

Figure 8 *J–R* curves of nanoclay-filled PP containing (●) 0 wt %, (▲) 10 wt %, (◇) 20 wt %, (×) 30 wt %, (□) 40 wt %, and (■) 50 wt % clay.

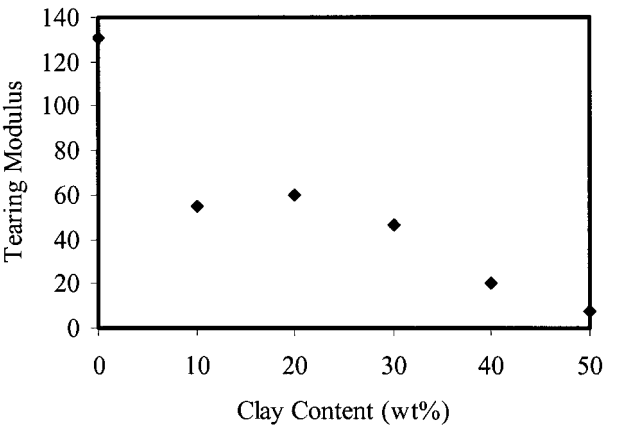

Figure 9 Tearing modulus of nanoclay-filled PP versus clay content.

a strengthening effect as demonstrated in Figures 4 and 5. However, the reduction in chain mobility (Fig. 6) continues to allow a significant increase in resistance as a crack advances (Figs. 8 and 9). The debonding at the polymer–clay interface at the point of fracture appears to promote some closure forces around the wake of a crack, which produces the observed crack growth resistance. Future work will focus on lower clay content from between 1 and 10 wt % for practical applications and the sequence of events as a crack advances using microscopic techniques.

CONCLUSIONS

MAPP was blended with organoclay using conventional extrusion methods. The gallery spacing was shown to enlarge during melt compounding followed by recompounding, but injection molding virtually wiped out the thermal history due to extrusion and thereby distinctive peaks were once again observed in XRD. Strength and stiffness increased with an increase in the clay content, in general, but the fracture deformation showed a transition from ductile to brittle fracture. As a result, the *J*-integral fracture initiation toughness decreased as the clay loading increased. The reduction in ductility and toughness was attributed to the constrained mobility of polymer chains in the presence of nanoclay particles. However, the constraint in chain mobility sufficed to allow substantial development in crack-propagation resistance interpreted using the initial slopes of the *J–R* curves and the tearing modulus concept. SEM photomicrographs were consistent in showing ductile voiding and fibrous structures and featureless cleavage at relatively low and high loadings of clay, respectively.

The authors sincerely wish to thank Dr. T. Lan of Nanocor Inc. for supplying the modified montmorillonite for this study. Discussion and support from Prof. A. F. Yee and Dr.

C. B. He of the Institute of Materials Research and Engineering, Singapore, on the development of this project were greatly appreciated by the authors.

References

1. Nam, P. H.; Maiti, P.; Okamoto, M.; Kotaka, T.; Hasegawa, N.; Usuki, A. Polymer 2001, 42, 9633.
2. Kawasumi, M.; Hasegawa, N.; Kato, M.; Usuki, A.; Okada, A. Macromolecules 1997, 30, 6333.
3. Hasegawa, N.; Okamoto, H.; Kawasumi, M.; Kato, M.; Tsukigase, A.; Usuki, A. Macromol Mater Eng 2000, 280/281, 76.
4. Hasegawa, N.; Okamoto, H.; Kato, M.; Usuki, A. J Appl Polym Sci 2000, 78, 1918.
5. Lan, T.; Qian, G. Q. In Proceedings of Additives '00, Clearwater Beach, FL, April 10–12, 2000.
6. Dennis, H. R.; Hunter, D. L.; Chang, D.; Kim, S.; White, J. L.; Cho, J. W.; Paul, D. R. Polymer 2001, 42, 9513.
7. Manias, E.; Touny, A.; Wu, L.; Strawhecker, K.; Lu, B.; Chung, T. C. Chem Mater 2001, 13, 3516.
8. Hasegawa, N.; Kawasumi, M.; Kato, M.; Usuki, A.; Okada, A. J Appl Polym Sci 1998, 67, 87.
9. Kato, M.; Usuki, A.; Okada, A. J Appl Polym Sci 1997, 66, 1781.
10. Lee, J. W.; Lim, Y. T.; Park, O. O. Polym Bull 2000, 45, 191.
11. Kim, K. N.; Kim, H.; Lee, J. W. Polym Eng Sci 2001, 41, 1963.
12. Garces, J. M.; Moll, D. J.; Bicerano, J.; Fibiger, R.; McLeod, D. G. Adv Mater 2000, 12, 1835.
13. Zerda, A. S.; Lesser, A. J. J Polym Sci Polym Phys 2001, 39, 1137.
14. Li, Y.; Wei, G.-X.; Sue, H.-J. J Mater Sci 2002, 37, 2447.
15. Mai, Y.-W.; Wong, S.-C.; Chen, X.-H. In Polymer Blends, Vol. 2: Performance; Paul, D. R.; Bucknall, C. B., Eds.: Wiley-Interscience: New York, 2000; Chapter 20.
16. Pinnavaia, T. J.; Lan, T.; Wang, Z.; Shi, H. Z.; Kaviratna, P. D. In Nanotechnology; Timp, G.-L., Ed.; Springer: New York, 1999; Chapter 17.
17. Zhang, Q.; Fu, Q.; Jiang, L. X.; Lei, Y. Polym Int 2000, 49, 1561.
18. Kojima, Y.; Usuki, A.; Kawasumi, M.; Okada, A.; Fukushima, Y.; Karauchima, T.; Karauchi, T.; Kamigaito, O. J Mater Res 1993, 8, 1185.
19. Reichert, P.; Nitz, H.; Klinke, S.; Brsch, R.; Thomann, R.; Mulhaupt, R. Macromol Mater Eng 2000, 275, 8.
20. Ma, J. S.; Qi, Z. N.; Hu, Y. L. J Appl Polym Sci 2001, 82, 3611.
21. Zanetti, M.; Camino, G.; Reichert, P.; Mulhaupt, R. Macromol Rapid Commun 2001, 22, 176.
22. Zanetti, M.; Camino, G.; Canavese, D.; Morgan, A. B.; Lamelas, F. J.; Wilkie, C. A. Chem Mater 2002, 14, 189.
23. Gilman, J. W.; Jackson, C. L.; Morgan, A. B.; Harris, R., Jr.; Manias, E.; Giannelis, E. P.; Wuthenow, M.; Hilton, D.; Phillips, S. H. Chem Mater 2000, 12, 1866.
24. Oya, A.; Kurokawa, Y.; Yasuda, H. J Mater Sci 2000, 35, 1045.
25. Messersmith, P. B.; Giannelis, E. P. J Polym Sci Part A Polym Chem 1995, 33, 1047.
26. Murase, S.; Inoue, A.; Miyashita, Y.; Kimura, N.; Nishio, Y. J Polym Sci Part B Polym Phys 2002, 40, 479.
27. LeBaron, P. C.; Wang, Z.; Pinnavaia, T. J. Appl Clay Sci 1999, 15, 11.